Science Advances
AAAS
Manuscript Template

FRONT MATTER

Title
- Shock-recovered maskelynite indicates low-pressure ejection of shergottites from Mars.
- Low shock pressure in Martian meteorites.

Authors
Jinping Hu[1*], Paul D. Asimow[1], Yang Liu[2], Chi Ma[1]

Affiliations
[1]Division of Geological and Planetary Sciences, California Institute of Technology, Pasadena, CA 91125, USA.
[2]Jet Propulsion Laboratory, California Institute of Technology, Pasadena, CA 91109, USA.
*corresponding author. Email: jinping@caltech.edu

Abstract
Diaplectic feldspathic glass, commonly known as maskelynite, is a widely-used impact indicator, notably for shergottites, whose shock conditions are key to their geochemistry and launch mechanism. However, classic reverberating shock-recovery experiments show maskelynitization at higher shock pressures (>30 GPa) than the stability field of the high-pressure minerals found in many shergottites (15-25 GPa). Most likely, differences between experimental loading paths and those appropriate for Martian impacts have created this ambiguity in shergottite shock histories. Shock-reverberation yields lower temperature and deviatoric stress than single-shock planetary impacts at equivalent pressure. Here, we report the Hugoniot equation of state of a Martian analogue basalt and single-shock recovery experiments, indicating partial-to-complete maskelynitization at 17-22 GPa, consistent with the high-pressure minerals in maskelynitized shergottites. This pressure explains the presence of intact magmatic accessory minerals, used for geochronology in shergottites, and offers a new pressure-time profile for modeling shergottite launch, likely requiring greater origin depth.

Teaser
Experiments on shock amorphization of plagioclase in Mars-like basalt reconcile the pressure scale for martian meteorites

MAIN TEXT

Introduction
The feldspar-to-maskelynite transformation is one of the most widely observed shock-metamorphic features in impacted rocks (*1*). Although the original 19th century identification of maskelynite in the Shergotty meteorite as a new mineral was inaccurate because of the shortcomings of 19th century analytical techniques (*2*, *3*), the term has subsequently come to describe isotropic feldspathic glass created by pressure-induced solid-state transformation (diaplectic glass) (*4*), whereas quenched feldspathic melt is empirically referred to as normal

glass. The shock pressure (P)-temperature (T)-pulse duration (t) conditions indicated by the formation and preservation of maskelynite offer essential constraints on the thermal (*5*) and launch history (*6–8*) of shergottites, a subgroup of Martian meteorites in which plagioclase is always partially or fully maskelynitized, supposedly due to the shock experienced during impact-driven acceleration to the escape velocity of Mars (*9*, *10*).

The shock conditions required for maskelynitization have been investigated in shock-recovery experiments (*4*, *11–15*). These studies converge on a range from 26 to 32 GPa as the threshold for partial to complete amorphization of calcic plagioclase (*9*) (Fig. 1). Yet shock pressures exceeding 30 GPa for maskelynitized shergottites are inconsistent with the increasing recognition that their high-pressure (HP) mineral assemblages have stability fields limited to <25 GPa (*16*, *17*). Moreover, shock pressure substantially above 30 GPa is expected to enhance local melting (*18*) and cause transformation and reversion of baddeleyite to and from HP polymorphs with the potential for Pb loss (*19*, *20*). That may be inconsistent with the magmatic crystallization U-Pb ages commonly recorded by untransformed baddeleyite grains found directly adjacent to maskelynite in shergottites (*5*). This discrepancy remains an impediment to understanding the shock disturbances and launch process experienced by shergottites. More nuanced compression studies show that peak pressure, pulse duration, temperature, strain rate and deviatoric stress are all important factors affecting maskelynitization (*21–24*). Full amorphization of calcic plagioclase requires 32 GPa in 20 ns laser shocks (*24*) but <10 GPa in longer-pulse, shockless rapid compression (*23*). Hence, if the presence of maskelynite is to offer an accurate peak pressure for shergottites, the thermobarometer needs to be based on experiments that resemble, as closely as possible, the P (pressure)-T (temperature)-t (time)-$\dot{\epsilon}$ (strain rate) path associated with natural impacts into shergottite-like targets on Mars.

In natural impacts, initial loading to high pressure commonly occurs in a single step from ambient to Hugoniot conditions (*25*). Two-wave loading due to phase transitions or shock reflections from impedance contrasts (like metal grains) is possible but should be localized (*26*). Multi-step loading to peak pressure is rare in nature and was not the path leading to pervasive maskelynite in shergottites. However, classic shock-recovery experiments commonly utilize multiple shock reflections across a low-impedance sample embedded in a high-impedance chamber, whereby the sample “rings up” to a peak pressure equal to the shock pressure in the chamber material (Fig. S1). The advantage of this reverberation technique is that peak pressure in the sample is independent of the sample’s Hugoniot equation of state (EoS), which may be unknown and complex to model. However, loading to a given peak pressure by reverberation also results in lower energy, temperature and deviatoric stress than single-shock loading, thereby differing from the P-T-t-$\dot{\epsilon}$ path of natural shocks and making it harder to produce pronounced shock metamorphism (*27*). This may be the primary cause of the pressure gap between the threshold for maskelynite formation in experimentally shock-recovered samples and in naturally impacted shergottites (*9*, *17*). Moreover, many previous experimental studies used plagioclase single crystals (*12*, *13*) as starting materials. Single crystals have zero porosity and follow a lower-temperature path than likely target materials on Mars, where shock melt pockets record at least local high temperatures (*28*). In this study, we develop a new shock-recovery setup to generate well-defined single-shock loading paths, resembling the P-T-t-$\dot{\epsilon}$ path of natural impacts on Mars. Based on results from a Mars rock simulant (a slightly porous natural basalt), we propose an improved calibration of the maskelynitization conditions in shergottites.

Results and Discussion

Hugoniot EoS of basalt

To approach shock conditions matching shergottites, we used Saddleback basalt, the source of Mojave Mars Simulant (*29*), which is rich in phenocrysts of An_{65} labradorite (Table S1). To design recovery experiments that achieve single-shock loading and to know the pressure precisely in such experiments, we measured the Hugoniot EoS of Saddleback basalt (Fig. 2; Methods), i.e. the family of shock states achieved by shocks of varying strength into this starting material. The shock velocity (U_s) and particle velocity (u_p) of Saddleback basalt were measured using the inclined mirror technique (see Methods); the data are shown in pressure-volume (P-V) space in Fig. 2.

In the absence of phase change or elastic-plastic transition during shock, the U_s-u_p Hugoniot is empirically linear and the P-V Hugoniot is derivable. In contrast, Saddleback basalt shows a fast low-pressure (LP) wave and a slow high-pressure (HP) wave (Fig. 2c), interpreted to be a density transition to a denser state. That results in a piecewise Hugoniot with LP, HP, and mixed regimes (Fig. 2c). The density transition occurs in the range of 15.4 to 16.6 GPa. Although not all published Hugoniots of basalts show this transition clearly, a phase change is observed in Kinosaki basalt at 13-18 GPa (*30*). Even in a study that found final shock states along a nearly-linear Hugoniot (*31*) (Fig. 2c), time-resolved wave velocities indicate stepped pressure rise and complex wave structures in this range (Fig. S3). Our experimental determination of the Hugoniot EoS of Saddleback basalt enables precise interpretation of shock pressures in our recovery experiments.

Shock-recovered maskelynite in basalt

Seven recovery experiments span the transition between density regimes along the Hugoniot (Table S3). For three single/double-shock experiments, we employed sample/flyer thickness ratios greater than 2 to prevent reverberation (see Methods); this allows time for at most one shock reflection to partially transit the sample before a release wave arrives to attenuate the shock. The sample region that released after only one shock transit and the region that released after one shock reflection can be identified unambiguously in this geometry (Fig. 3A).

S1240 is the shot with the lowest impact velocity. The front of the sample experienced a single loading pulse to 15.8 GPa, maintained for 1.8 μs before release wave arrival (Fig. S5). The single-shocked central front area of the recovered sample contains almost all birefringent plagioclase (Fig. 3B) and shows a white color in thick section (Fig. 3A). The back of the sample in the same experiment experienced one reshock from the steel back-wall and reached 21.7 GPa. This reshocked area displays isotropic maskelynite (Fig. 3B) and transparent grains in thick section (Fig. 3A). The visual boundary between zones of amorphized and crystalline plagioclase is plainly visible in both thin and thick section (dashed line in Fig. 3A-3B) and coincides with the intersection of the reshock with the release wave.

Two more recovery experiments help to refine the nature of the glass transition upon single- and double-shock loading. S1244 captures the onset of partial maskelynitization in the front single-shock region at 17.4 GPa (Fig. 3C). Multiple plagioclase grains in this region are divided into areas that are isotropic and areas that display curved twin planes and low birefringence (Fig. 3C). All plagioclase grains in the reshocked region (peak pressure 29.2 GPa) are amorphized. The corners of the capsule, which experience edge effects and strong shear heating, contain complete maskelynite that formed at poorly known P-T conditions somewhat different than the central part (Fig. S6). S1245, with slightly higher impact velocity and peak pressure of 19.3 GPa in the single-shock region, shows a noticeably higher degree of partial maskelynitization than S1244.

Some large (~500 μm) feldspathic domains are completely isotropic and other plagioclase grains show very low birefringence that makes twinning unobservable. Most feldspar domains look transparent in thick section (Fig. S7), resembling the fully maskelynitized regions in other recovered samples (e.g. Fig. 3A). To ensure the correct identification of weakly birefringent plagioclase, we employed electron back-scatter diffraction (EBSD) to map out feldspathic domains with diffraction patterns (Fig. S7). Diffraction band-contrast maps of S1245 indicate that some feldspar domains in the back of the single-shock region, whose shock pulse is 0.5 μs shorter than that of the sample front (Fig. S5), still retain some level of crystalline structure, despite showing very low birefringence in cross-polarized light. In both S1244 and S1245, the single-shock regions contain scarce instances of glass displaying flow and schlieren features, presumed to be quenched from local melting of plagioclase (plus some pyroxene). This feldspathic normal glass shows notably lower fracture density than the surrounding maskelynite or plagioclase (Fig. S6 and S7), indicating viscous relaxation of shear stress before shock release.

The results of the three thick-sample recovery shots spanning the glass-transition interval along the Hugoniot demonstrate the onset of maskelynitization occurs around 17 GPa, with maskelynite becoming predominant above 19 GPa and complete transition by 22 GPa. The pressures are slightly higher than the transition point in the Hugoniot (Fig. 1), likely because some excess pressure is needed to preserve the amorphization upon recovery (*24*, *32*). The onset pressure of maskelynitization for single shocks of our target material is 17 GPa, much lower than the 25-27 GPa in reverberation experiments (Fig. 1). Our thin-sample experiments replicated previous results, showing that reverberation causes complete maskelynitization of Saddleback basalt at around 30 GPa or above (Table S3 and Fig. S8).

Low shock-pressure and temperature of shergottites

The pressure threshold for conversion of plagioclase to maskelynite is not a simple function of peak pressure but depends on the P-T-t-$\dot{\epsilon}$ loading path (*21*, *23*, *24*). Evaluation of the peak pressure of shergottites therefore requires experiments that approach the conditions of natural impacts on Mars. Unfortunately, natural impacts, laboratory shocks (propellant- or laser-driven), static and rapid compression experiments all populate different regimes in P-T-t-$\dot{\epsilon}$ space. Planetary impacts related to shergottites are thought to involve pulses of 10^{-3} to 10^{-2} s duration and strain rates greater than ~10^5 s^{-1} (*17*, *33–35*). Reproducing that duration and strain rate simultaneously is challenging. Shock recovery experiments provide the correct strain rate but a shorter pulse duration, <10^{-5} s (Fig. S5), whereas anvil compression provides longer pulse durations but much lower strain rates, <10^{-1} s^{-1} (*21*, *23*). Our propellant shock experiments with microsecond pulses demonstrate maskelynitization pressures intermediate between estimates from laser shocks of 20 ns duration (*24*) and anvil compression experiments lasting at least seconds (*23*), suggesting a negative correlation between transformation pressure and pulse duration. Therefore, the pressure thresholds (17.4-21.7 GPa) observed in our experiments are probably slightly higher than the actual pressure of partially maskelynitized shergottites (Fig. 3D) launched by Martian impacts. In other word, our experiments set a new upper bound for the maskelynitization of calcic plagioclase in natural impacts. This upper bound also applies to most terrestrial impact sites, whose pulses last >10^{-3} s.

Increasing temperature favors maskelynite formation at lower pressure. Static compression experiments observe this effect (*21*) (Fig. 1). Likewise, preheating of basalt to 1073 K lowers the threshold for partial maskelynitization in reverberation experiments from >26 GPa to ~22 GPa (*36*). The higher shock temperatures achieved by single shocks compared to previous reverberation-shock paths might therefore explain the observation of maskelynite formation at ~17 GPa. However, calculated shock temperatures for single-shock and reverberating shock loading paths (Fig. 1A) are negligibly different in the range where we find the onset of maskelynite formation, becoming more different only above 30 GPa. Although one-step loading of a target with the appropriate porosity does offer a better match to the shock temperatures experienced by shergottites than reverberation-shocking single crystals, temperature does not appear to solely explain the dramatically lower maskelynitization threshold in our experiments compared to reverberation studies.

Another key difference between single and reverberating shock loading is the magnitude of deviatoric stress experienced by the sample. Reverberating shocks that peak at 25-30 GPa typically have first shock fronts with pressure amplitudes of ~10 Gpa that overdrive the Hugoniot Elastic Limit (HEL, ~5 Gpa) by about 5 Gpa before material failure (*37*). It is likely that subsequent shocks raise the pressure in a nearly hydrostatic fashion without material strength effects and cause limited increases in deviatoric stress. In contrast, a single shock directly to the peak pressure creates transient deviatoric stress several times larger by overdriving the HEL more strongly (*38*). Large deviatoric stresses are likely to facilitate low-pressure maskelynitization (*39*). Hydrocode simulation also shows that shear stress varies temporally and spatially for regions of the same peak pressure during impact cratering, which plays an important role in producing meter-scale features such as shutter cones (*40*). Hence, the single-shock experiments better resemble this aspect of the P-T-t-$\dot{\epsilon}$ path of Martian impacts. In an actual planetary impact, the longer duration (*33*), shock turbulence (*41*) and extensive shear flows (*42*) may all contribute to further lowering the pressure threshold for maskelynitization.

Raman spectra of feldspars in shergottites demonstrate broadening of diagnostic peaks with increasing shock and maskelynitization level (*10*, *43*). The pressure associated with such peak broadening has been calibrated using reverberating shock experiments and assigned to shock pressures of 26 to >45 GPa. However, this spectroscopic shock level barometer, like the maskelynite threshold, likely requires a systematic pressure shift to account for the differences between natural shock loading and reverberation experiments (*43*).

The HP mineral assemblages in many fully maskelynitized shergottites, such as Tissint, Zagami and DaG 735, are stable at <25 GPa in basaltic bulk compositions (*16*) (Fig. 1). In distinct contrast, these shergottites mostly contain full maskelynite with no birefringent plagioclase, which has been assigned to pressure >30 GPa on the basis of previous reverberation shock experiments (Fig. 1). This discrepancy is problematic — if all the shergottites were truly shocked beyond 30 GPa, then post-spinel transformation, recrystallization and local melting would be pervasive. Although complete maskelynitization sets a lower bound of shock pressure in shergottites, more heavily shocked rocks such as ALH 77005 and NWA 1950 that reached 35-40 GPa (*18*, *44*) commonly contain brown olivine with shock-induced planar deformation features (*36*) and quenched vesicular feldspathic glass instead of maskelynite (Fig. 1B; Fig. S10). These textures are reproduced by the extensive deformation and melting (Fig. S8) observed in one of our higher-pressure experiments (S1238, 42.4 GPa). The potential HP minerals in these strongly-shocked rocks are likely annealed (*25*), resulting from post-shock temperature high enough for retro-metamorphism, in contrast to the maskelynitized shergottites shocked to <25 GPa. Even for the rare examples of partially maskelynitized shergottites, such as NWA 8159 (*17*) (Fig. 3), the previously determined threshold pressure was still above 25 GPa (Fig. 1). Our single-shock recovery experiments reproduce partial maskelynite textures like those in NWA 8159 (Fig. 3C-3D; Fig. S10) and yield a new partial-to-complete maskelynitization threshold, 17.4-21.7 GPa, that is consistent with the majorite-pyroxene assemblage in the same meteorite (*17*) (Fig. 1). Based on new pressure thresholds, the pressure of <25 GPa inferred from HP phase assemblages of shergottites that reached the onset of post-spinel transformation, such as Zagami and Tissint, are therefore sufficient for the observed complete maskelynitization.

The new low-pressure maskelynitization threshold is also more consistent with untransformed accessory minerals in shergottites, such as baddeleyite (*5*). Zircon and baddeleyite undergo several displacive transitions with low activation energy and fast kinetics (*19*, *20*), allowing transition at low temperature (*45*). Previous maskelynitization barometry indicated shock compression above 30 GPa and 600 °C bulk temperature in shergottites (Fig. 1). Such conditions should have caused pervasive transformation of baddeleyite to orthorhombic and tetragonal structures, followed by reversion to polycrystalline monoclinic aggregates upon release, as observed in terrestrial target rocks that experienced similar long-pulse impact events. The neighborhoods around plagioclase crystals likely experience local temperature even higher than the bulk rock (*27*), due to the compressibility of feldspar and the volume decrease associated with maskelynite formation (Fig. 1A and 2C). In fact, martian baddeleyite can be found entrained in fully maskelynitized feldspar in shergottites and retains magmatic crystallinity, zoning patterns, and U-Pb ages, which has previously been seen as inconsistent with peak shock pressure > 30 GPa (*46*). The lower maskelynization pressure, 17.4-21.7 GPa, in our study is compatible with these undisturbed zirconium minerals. Although the mechanism of Pb loss during shock deformation and ZrO_2 transformation is not fully understood (*47*), moderate values of shock pressure, shock temperature and post-shock temperature, in association with our new maskelynitization threshold are more consistent with the observed crystallography and limited resetting of the zircon and baddeleyite. In turn, this result strengthens the case that the <0.6 Ga ages of shergottites are primary crystallization ages and not partially reset values.

Launch of shergottite from greater depth

Finding agreement between the peak pressures implied by feldspar transformation and those recorded by HP minerals crystallized in melt veins also eliminates the need for complex partial release scenarios featuring an excess pressure spike (for maskelynitization) followed by a stable shock pulse (for HP minerals). Instead, a unified shock pressure of <25 GPa for maskelynite and HP minerals in many shergottites favors models in which the melt veins record plateau conditions at peak pressure lasting 10-100 ms (*17*, *33*, *34*). Thus, the whole *P-t* profile extracted from analysis of shergottites becomes simple and well-constrained and potentially more suitable for modeling the launch of shergottites from Mars.

Because particle velocity of several km s^{-1} corresponds to excessive pressure close to whole rock melting, impact spallation models are proposed for accelerating Martian meteorites to escape velocity while limiting the intensity of shock metamorphism that they experience (*6*, *7*). Kurosawa et al. (*7*) extracted pressure and velocity histories of multiple tracers in hydrocode spallation simulations and demonstrated that ejection from depth 1-2% of the impactor radius is most probable for achieving escape with a plateau-like *P-t* profile. Although their modeled impactor of 10 km radius corresponds to a very large crater, the same scaled depth in the case of a smaller impactor would still be consistent with the absolute depth needed to explain the differences noted between Martian meteorites and surficial lithologies (*48*) and with the absence of 2π irradiation (*49*). By contrast, in previous scenarios requiring multistage *P-t* histories, ejecta likely originate at depth <0.5% of the impactor radius. In such models, satisfying the absolute depth, pulse duration, and pressure constraints requires an impactor of several km radius and crater diameter >100 km (*8*). Such a crater size is even greater than the largest candidate craters for the origin of the shergottites, like Mojave (58 km) and Kotka (29 km) (*50*).

Bowling et al. (*8*) demonstrate that there is a correlation between impact size and dwell time at a given pressure. Quantitatively, for a peak pressure of ~30 GPa, launched material has a ratio of HP dwell time to impactor radius of up to 20 μs m^{-1}, whereas for 20 GPa peak pressure this ratio decreases to <15 μs m^{-1}. Hence ejection at peak pressure of ~20 GPa rather than 30 GPa implies a 30% larger impactor for the same dwell time (Fig. S11). One remaining issue here is that peak pressure may increase to >30 GPa in material ejected from greater depth close to the impact center. Elliot et al. (*48*) applied a fragmentation model in their simulations and found that a 20 m layer of tuff on top of basalt enhances the overall ejection capability of a 1 km impactor, compared to pure basalt targets, potentially launching material from depth to escape at a lower peak pressure. In sum, somewhat counterintuitively, a decrease in the estimate of peak pressure recorded by the shergottites implies an increase in diameter of the crater from which they were ejected. Low-pressure ejection increases the need for special geometries of oblique impact and for mechanisms such as ejecta pileup recognized in recent high-resolution simulations (*7*). In turn, a decrease in the estimate of shock pressure in the shergottites increases the rarity of ejection of unmelted rocks and increases the probability that the known shergottites were ejected by fewer impact events, given their narrow range of cosmic ray exposure ages (*51*). Low-pressure maskelynitization combined with HP mineral stability fields indicates that future hydrocode simulations of shergottite launch should focus on a plateau-like *P-t* profile and increased depth of origin.

Because maskelynitization of feldspar depends on many variables, including mineral composition, target porosity, and the P-T-t-$\dot{\epsilon}$ path of shock compression, it is important to calibrate shock conditions with suitable experiments. The high deviatoric stress, high strain rate and well-defined shock temperature realized in a one-step shock-loading setup are appropriate for interpreting shocked meteorites from impacts on Mars and other basaltic targets like Vesta and the Earth. The methodology of EoS measurement combined with single-shock recovery experiments can be applied to terrestrial basalts, HEDs and lunar rock analogues to better constrain the pressure of the maskelynitized rocks in their corresponding groups.

Materials and Methods

Martian analogue sample

To reproduce the shock conditions in shergottites, we used Saddleback basalt (Table S1-S2) from the Mojave Desert in southern California (*29*). This nearly holocrystalline basalt, with low porosity (3%) and <10% groundmass, was selected for testing the mechanical design of the Curiosity rover (the Mojave Mars Simulant), because of the similarity of its physical properties to Martian rocks (*29*).

Hugoniot measurement in shock experiments

The Hugoniot EoS of material is most commonly expressed as an empirical linear (or piecewise-linear) relationship $U_s = C_o + su_p$, where U_s and u_p are the velocity of the shock front and the particle velocity in the shocked material; C_o is expected to be the zero-pressure bulk sound speed and s is a dimensionless factor related to the pressure derivative of the bulk modulus. Knowing the U_s-u_p relationship for each material involved in an experimental impact, one can calculate the shock-state pressure and volume (V) via the Rankine-Hugoniot conservation equations and the assumption of velocity and stress continuity across interfaces. With additional constraints on the isochoric heat capacity and thermodynamic Grüneisen parameter, the temperature increases across a shock can also be estimated (*25*) (Fig. 1; supplementary section S1 and S5).

The basalt EoS shots were performed on the 40 mm propellant gun in the Caltech Lindhurst Laboratory for Experimental Geophysics. More details of experimental setup are in supplementary section S1. Shock arrivals at the silvered surface of each mirror generate sharp cutoffs on the Hadland Imacon 790 streak-camera image (Fig. 2B). The travel time of the shock wave across the sample is determined by the average of the time differences between the light cutoffs at the two sample flat mirrors and at the adjacent driver plate mirrors (t_1-t_0 in Fig. 2B), converted to travel time and then shock-wave speed (U_s). The impedance match solution (which imposes continuity of particle velocity and normal stress at the driver-sample interface), the known Hugoniot of the driver, and the measured U_s yield the sample particle velocity u_p.

Assuming the pre-shock velocity of the sample is zero, the Rankine-Hugoniot equations for conservation of mass, momentum and energy (E) across the shock front can be written as:

$$\rho_o U_s = \rho (U_s - u_p) \qquad (1a)$$

$$(P - P_o) = \rho_o U_s u_p \qquad (1b)$$

$$E - E_o = (P + P_o)(V - V_o)/2 \qquad (1c)$$

These equations allow calculation of P, ρ, and $(E - E_o)$ in the shock state given measurements of U_s, u_p, and initial density ρ_o. In the case of a two-wave structure, the high-pressure slow wave also follows the impedance match at driver-sample interface.

When the target material undergoes an elastic-plastic or low-density to high-density transition, a two-wave structure forms, whereby the slower second wave has a higher pressure. In this case, only the arrival of the faster first wave can be captured by the streak camera, but the impedance match at the driver-sample interface needs the P, U_s and u_p of the second wave. For such cases, we measure the slow wave and fast wave(s) by adding an inclined mirror behind the sample at an angle ϕ, in addition to the regular flat mirrors on the driver and basalt sample disc (Fig. 2A). The inclined mirror is wedge-shaped to so that its refraction and reflection offsets cancel out and light is reflected back to the center of the camera sensor. When a shock wave arrives at the rear free surface of the sample, decompressed material traverses the vacuum at free-surface velocity U_{fs} and hits the inclined mirror, creating an oblique cutoff (γ in Fig. 2B) along the inclined-mirror streak. U_{fs} is determined from the corresponding angle γ on the streak cutoff using

$$U_{fs} = (W \cdot \tan\phi) / (m \cdot \tan\gamma) \qquad (2)$$

where W and m are the writing rate and magnification of the streak image, respectively(*37*). Thus, the arrival of the second wave, with higher u_p and U_{fs} than the first wave, is shown by the change in γ angle on the streak cutoff (t_2 in Fig. 2B). Assuming the release adiabat is exactly a reflected Hugoniot, U_{fs} is expected to be 2^*u_p (supplementary section S1). The timing of the slope transition also approximately indicates the second wave velocity by

$$U_{s2} = (d+(t_2-t_1)^*U_{fs1})/(t_2-t_0) \qquad (3)$$

where d is the sample thickness and the meaning of each time t_i is indicated on Figure 2B. In the case that $U_{fs} \neq 2u_p$, which is common for a wave in a transformed phase, the final particle velocity can be calculated by iteration between U_{s2} and the impedance match solution at the sample-driver interface (Fig. S1).

In our first two EoS shots (1123 and 1124), we observed U_s decreasing from 6136 m s^{-1} to 5232 m s^{-1} as flyer velocity U_{fp} increases from 1394 m s^{-1} to 1598 m s^{-1} (Fig. S2), indicating that in this range the sample undergoes a density transition to a higher density state that produces a two-wave structure; the slower, higher-pressure wave is not captured by the flat mirror streak cutoffs.

To determine U_s and u_p for both the first and second wave, the third shot (1126), fired at an intermediate U_{fp} of 1479 m s^{-1}, employed an inclined-mirror method to measure multiple wave velocities. The first wave has U_{s1} = 5766 m s^{-1} and u_{p1} = 1009 m s^{-1}, whereas the second and final wave has U_{s2} = 5232 m s^{-1} and u_{p2} = 1297 m s^{-1}. Interpreting this two-wave structure as recording a density transition, we find that the density transition is complete at 16.6 GPa, (much higher than the Hugoniot elastic limit (HEL), which can generate a similar two-wave structure in weaker shocks). The data from all three EoS shots can be summarized by a piecewise-linear fit, with negative slope $U_s = 9594 - 3.72u_p$ for u_p between 900 and 1200 m s^{-1} and a high-density phase at $u_p \geq 1200$ m s^{-1} characterized by $U_s = 3603 + 1.256u_p$. The transition pressure interval extends from 15.4 to 16.6 GPa and results from incomplete density transition and mixing of low- and high-density states along the Hugoniot. The EoS shots are summarized in Figure S2 and Table S3. These fits are sufficient to enable calculation of pressures in our recovery experiments. The low-pressure Hugoniot is estimated (Fig. 2c) using the zero-pressure sound speed of Saddleback basalt[27] and does not affect the pressure calculation of recovery experiments (Fig. S2). Comparison among Hugoniots from Saddleback basalt and other feldspar rocks is discussed in the supplementary section S2.

Shock recovery experiments

Discs of Saddleback basalt with a diameter of 5 or 7.6 mm and thickness d_{sample} of 1.0 to 5.0 mm were used for total of 7 shock recovery experiments. The samples were embedded in 304 stainless steel (SS304) chambers and impacted by tantalum flyer plates of thickness d_{flyer} from 1.5 to 2.1 mm (Table S3; supplementary section S3). In practice, a thickness ratio $d_{sample}/d_{flyer} < 1$ allows enough shock transits across the sample and chamber to effectively achieve an ultimate peak pressure by reverberation, before the rarefaction wave from the back of the flyer arrives. In 4 out of the total 7 recovery shots, the sample experienced full reverberation to peak pressures from 33 to 42 GPa after first shock pressures from 16 to 19 GPa (Table S3 and Fig. S5). Three more recovery shots with similar impact velocities and $d_{sample}/d_{flyer} > 2$ were performed. In this geometry, wave propagation calculations show that the front portion of the sample is shocked only once before release, to the same range of initial pressures, 16-19 GPa. In each of these three non-reverberating experiments, some part of the sample near the steel back wall also experienced one reflected shock (Fig. 3; Figs. S5-S8).

The impacted target assemblies were cut parallel to the impact direction into two equal halves. One half was polished into a thick section for reflected light imaging. The other half was sliced and mounted in Petropoxy 154 to make a standard 30 µm thin section for examination in cross-polarized transmitted light. Both thick and thin sections were analyzed with a Zeiss 1550VP field emission scanning electron microscope in the Division of Geological and Planetary Sciences at Caltech. Backscattered and secondary electron (BSE and SE) images are employed to observe the micro-textures of the shocked basalt. Energy dispersive X-ray spectroscopy (EDS) with an Oxford X-max silicon drift detector was used to measure the chemical composition at 15 kV accelerating voltage and 4-6 nA beam current, achieving more than 200 counts/channel and 40% dead time. We also employed electron backscatter diffraction (EBSD) to investigate the crystallinity of shocked minerals. Regions with resolved diffraction bands were indexed with mean angular deviation (MAD) values less than 0.8° (Fig. S7). Regions showing no resolvable diffraction bands are considered amorphous. The band contrast metric quantifies the degree of crystallinity at the EBSD point analysis. Quantitative chemical analyses of rock-forming minerals and glasses were performed using a JEOL 8200 electron microprobe (WDS: 15 kV; 5-10 nA; beam in focused mode) interfaced with the Probe for EPMA program from Probe Software, Inc. Standards for these analyses were synthetic fayalite (Si*Kα* for olivine, Fe*Kα*), Shankland forsterite (Mg*Kα*), synthetic Mn_2SiO_4 (Mn*Kα*), synthetic anorthite (Al*Kα*, Si*Kα* for feldspar, Ca*Kα*), Amelia albite (Na*Kα*), Asbestos microcline (K*Kα*), synthetic TiO_2 (Ti*Kα*), and synthetic Cr_2O_3 (Cr*Kα*). Quantitative elemental microanalyses were processed with the CITZAF correction procedure (Table S1).

Because our impedance match calculations assume one-dimensional flow, we focused on the central portion of the sample when determining the abundance of completely or partially amorphized domains, to avoid regions affected by possible edge effects and rock-metal friction (Fig. S6). Although additional amorphous material commonly occurs along large fractures and at the capsule edges (Fig. 3A and Fig. S6), these are considered to be associated with edge conditions and are not considered when defining thresholds for maskelynite formation. The difference between maskelynitization thresholds obtained by shocking Saddleback basalt with those from other compression techniques is discussed in the main text and supplementary section S4.

References

1. A. E. Rubin, Maskelynite in asteroidal, lunar and planetary basaltic meteorites: An indicator of shock pressure during impact ejection from their parent bodies. *Icarus*. **257**, 221–229 (2015).

2. G. Tschermak, Die Meteoriten von Schergotty und Gopalpur. *Sitz-Ber. Akad. Wiss. Wien., math.-naturw. Kl., Abt. I*. **65**, 122–146 (1872).

3. L. Ferrière, F. Brandstätter, What is Maskelynite? Back to the Original Description and Thin Sections in Which it was First Described. *78th Annual Meeting of the Meteoritical Society.* 1856, 5184 (2015).

4. D. J. Milton, P. S. De Carli, Maskelynite: Formation by Explosive Shock. *Science*. **140**, 670–671 (1963).

5. D. E. Moser, K. R. Chamberlain, K. T. Tait, A. K. Schmitt, J. R. Darling, I. R. Barker, B. C. Hyde, Solving the Martian meteorite age conundrum using micro-baddeleyite and launch-generated zircon. *Nature*. **499**, 454–457 (2013).

6. J. N. Head, H. J. Melosh, B. A. Ivanov, Martian Meteorite Launch: High-Speed Ejecta from Small Craters. *Science*. **298**, 1752–1756 (2002).

7. K. Kurosawa, T. Okamoto, H. Genda, Hydrocode modeling of the spallation process during hypervelocity impacts: Implications for the ejection of Martian meteorites. *Icarus*. **301**, 219–234 (2018).

8. T. J. Bowling, B. C. Johnson, S. E. Wiggins, E. L. Walton, H. J. Melosh, T. G. Sharp, Dwell time at high pressure of meteorites during impact ejection from Mars. *Icarus*. **343**, 113689 (2020).

9. D. Stöffler, R. Ostertag, C. Jammes, G. Pfannschmidt, P. R. S. Gupta, S. B. Simon, J. J. Papike, R. H. Beauchamp, Shock metamorphism and petrography of the Shergotty achondrite. *Geochimica et Cosmochimica Acta*. **50**, 889–903 (1986).

10. J. Fritz, A. Greshake, D. Stöffler, Micro-Raman spectroscopy of plagioclase and maskelynite in Martian meteorites: Evidence of progressive shock metamorphism. *Antarctic Meteorite Research*. **18**, 96 (2005).

11. S. W. Kieffer, R. B. Schaal, R. Gibbons, R. Horz, D. J. Milton, A. Dube, Shocked basalt from Lonar Impact Crater, India, and experimental analogues. *Lunar and Planetary Science Conference Proceedings 7th*, 1391–1412 (1976).

12. R. V. Gibbons, T. J. Ahrens, Effects of shock pressures on calcic plagioclase. *Phys Chem Minerals*. **1**, 95–107 (1977).

13. R. Ostertag, Shock experiments on feldspar crystals. *J. Geophys. Res.* **88**, B364–B376 (1983).

14. J. R. Johnson, F. Hörz, Visible/near-infrared spectra of experimentally shocked plagioclase feldspars. *J. Geophys. Res.* **108**, 5120 (2003).

15. J. Fritz, V. Assis Fernandes, A. Greshake, A. Holzwarth, U. Böttger, On the formation of diaplectic glass: Shock and thermal experiments with plagioclase of different chemical compositions. *Meteoritics & Planetary Science*. **54**, 1533–1547 (2019).

16. N. Tomioka, M. Miyahara, High-pressure minerals in shocked meteorites. *Meteorit Planet Sci*. **52**, 2017–2039 (2017).

17. T. G. Sharp, E. L. Walton, J. Hu, C. Agee, Shock conditions recorded in NWA 8159 martian augite basalt with implications for the impact cratering history on Mars. *Geochimica et Cosmochimica Acta*. **246**, 197–212 (2019).

18. E. L. Walton, C. D. K. Herd, Dynamic crystallization of shock melts in Allan Hills 77005: Implications for melt pocket formation in Martian meteorites. *Geochimica et Cosmochimica Acta*. **71**, 5267–5285 (2007).

19. O. Ohtaka, H. Fukui, T. Kunisada, T. Fujisawa, K. Funakoshi, W. Utsumi, T. Irifune, K. Kuroda, T. Kikegawa, Phase relations and equations of state of ZrO2 under high temperature and high pressure. *Phys. Rev. B*. **63**, 174108 (2001).

20. L. F. White, J. R. Darling, D. E. Moser, C. Cayron, I. Barker, J. Dunlop, K. T. Tait, Baddeleyite as a widespread and sensitive indicator of meteorite bombardment in planetary crusts. *Geology*. **46**, 719–722 (2018).

21. T. Kubo, M. Kimura, T. Kato, M. Nishi, A. Tominaga, T. Kikegawa, K. Funakoshi, Plagioclase breakdown as an indicator for shock conditions of meteorites. *Nature Geosci*. **3**, 41–45 (2010).

22. A. R. Huffman, W. U. Reimold, Experimental constraints on shock-induced microstructures in naturally deformed silicates. *Tectonophysics*. **256**, 165–217 (1996).

23. M. Sims, S. J. Jaret, E.-R. Carl, B. Rhymer, N. Schrodt, V. Mohrholz, J. Smith, Z. Konopkova, H.-P. Liermann, T. D. Glotch, L. Ehm, Pressure-induced amorphization in plagioclase feldspars: A time-resolved powder diffraction study during rapid compression. *Earth and Planetary Science Letters*. **507**, 166–174 (2019).

24. A. E. Gleason, S. Park, D. R. Rittman, A. Ravasio, F. Langenhorst, R. M. Bolis, E. Granados, S. Hok, T. Kroll, M. Sikorski, T.-C. Weng, H. J. Lee, B. Nagler, T. Sisson, Z. Xing, D. Zhu, G. Giuli, W. L. Mao, S. H. Glenzer, D. Sokaras, R. Alonso-Mori, Ultrafast structural response of shock-compressed plagioclase. *Meteoritics & Planetary Science*. **57**, 635–643 (2022).

25. J. Hu, T. G. Sharp, Formation, preservation and extinction of high-pressure minerals in meteorites: temperature effects in shock metamorphism and shock classification. *Prog Earth Planet Sci*. **9**, 6 (2022).

26. J.-G. Moreau, T. Kohout, K. Wünnemann, Melting efficiency of troilite-iron assemblages in shock-darkening: Insight from numerical modeling. *Physics of the Earth and Planetary Interiors*. **282**, 25–38 (2018).

27. T. G. Sharp, P. S. DeCarli, "Shock effects in meteorites" in *Meteorites and the early solar system II*, D. S. Lauretta, H. Y. McSween Jr., Eds. (The University of Arizona Press, Tucson, 2006), 653–677.

28. Y. Liu, Y. Chen, Y. Guan, C. Ma, G. R. Rossman, J. M. Eiler, Y. Zhang, Impact-melt hygrometer for Mars: The case of shergottite Elephant Moraine (EETA) 79001. *Earth and Planetary Science Letters*. **490**, 206–215 (2018).

29. G. H. Peters, W. Abbey, G. H. Bearman, G. S. Mungas, J. A. Smith, R. C. Anderson, S. Douglas, L. W. Beegle, Mojave Mars simulant—Characterization of a new geologic Mars analog. *Icarus*. **197**, 470–479 (2008).

30. S. Nakazawa, S. Watanabe, M. Kato, Y. Iijima, T. Kobayashi, T. Sekine, Hugoniot equation of state of basalt. *Planetary and Space Science*. **45**, 1489–1492 (1997).

31. T. Sekine, T. Kobayashi, M. Nishio, E. Takahashi, Shock equation of state of basalt. *Earth Planet Sp*. **60**, 999–1003 (2008).

32. I. Daniel, P. Gillet, P. F. McMillan, G. Wolf, M. A. Verhelst, High-pressure behavior of anorthite: Compression and amorphization. *J. Geophys. Res.* **102**, 10313–10325 (1997).

33. P. Beck, P. Gillet, A. El Goresy, S. Mostefaoui, Timescales of shock processes in chondritic and martian meteorites. *Nature*. **435**, 1071–1074 (2005).

34. E. L. Walton, T. G. Sharp, J. Hu, J. Filiberto, Heterogeneous mineral assemblages in martian meteorite Tissint as a result of a recent small impact event on Mars. *Geochimica et Cosmochimica Acta*. **140**, 334–348 (2014).

35. J. Fritz, A. Greshake, High-pressure phases in an ultramafic rock from Mars. *Earth and Planetary Science Letters*. **288**, 619–623 (2009).

36. A. Takenouchi, T. Mikouchi, T. Kobayashi, T. Sekine, A. Yamaguchi, H. Ono, Fine-structures of planar deformation features in shocked olivine: A comparison between Martian

meteorites and experimentally shocked basalts as an indicator for shock pressure. *Meteoritics & Planetary Science*. **54**, 1990–2005 (2019).

37. T. J. Ahrens, V. Gregson Jr, Shock compression of crustal rocks: Data for quartz, calcite, and plagioclase rocks. *Journal of Geophysical Research*. **69**, 4839–4874 (1964).

38. N. K. Bourne, J. C. F. Millett, J. E. Field, On the strength of shocked glasses. *Proceedings of the Royal Society of London. Series A: Mathematical, Physical and Engineering Sciences*. **455**, 1275–1282 (1999).

39. F. Langenhorst, P. Joreau, J. C. Doukhan, Thermal and shock metamorphism of the Tenham chondrite: A TEM examination. *Geochimica et Cosmochimica Acta*. **59**, 1835–1845 (1995).

40. A. S. P. Rae, M. H. Poelchau, T. Kenkmann, Stress and strain during shock metamorphism. *Icarus*. **370**, 114687 (2021).

41. C. T. Adcock, O. Tschauner, E. M. Hausrath, A. Udry, S. N. Luo, Y. Cai, M. Ren, A. Lanzirotti, M. Newville, M. Kunz, C. Lin, Shock-transformation of whitlockite to merrillite and the implications for meteoritic phosphate. *Nat Commun*. **8**, 14667 (2017).

42. A. Greshake, J. Fritz, U. Böttger, D. Goran, Shear-induced ringwoodite formation in the Martian shergottite Dar al Gani 670. *Earth and Planetary Science Letters*. **375**, 383–394 (2013).

43. S. Shkolyar, S. J. Jaret, B. A. Cohen, J. R. Johnson, O. Beyssac, J. M. Madariaga, R. C. Wiens, A. Ollila, S. Holm-Alwmark, Y. Liu, Identifying Shocked Feldspar on Mars Using Perseverance Spectroscopic Instruments: Implications for Geochronology Studies on Returned Samples. *Earth Moon Planets*. **126**, 4 (2022).

44. E. L. Walton, S. P. Kelley, C. D. K. Herd, Isotopic and petrographic evidence for young Martian basalts. *Geochimica et Cosmochimica Acta*. **72**, 5819–5837 (2008).

45. H. Leroux, W. Reimold, C. Koeberl, U. Hornemann, J.-C. Doukhan, Experimental shock deformation in zircon: a transmission electron microscopic study. *Earth and Planetary Science Letters*. **169**, 291–301 (1999).

46. L. G. Staddon, J. R. Darling, W. H. Schwarz, N. R. Stephen, S. Schuindt, J. Dunlop, K. T. Tait, Dating martian mafic crust; microstructurally constrained baddeleyite geochronology of enriched shergottites Northwest Africa (NWA) 7257, NWA 8679 and Zagami. *Geochimica et Cosmochimica Acta*. **315**, 73–88 (2021).

47. T. Niihara, H. Kaiden, K. Misawa, T. Sekine, T. Mikouchi, U–Pb isotopic systematics of shock-loaded and annealed baddeleyite: Implications for crystallization ages of Martian meteorite shergottites. *Earth and Planetary Science Letters*. **341–344**, 195–210 (2012).

48. J. R. Elliott, H. J. Melosh, B. C. Johnson, The role of target strength on the ejection of martian meteorites. *Icarus*. **375**, 114869 (2022).

49. P. H. Warren, Lunar and Martian Meteorite Delivery Services. *Icarus*. **111**, 338–363 (1994).

50. A. Lagain, G. K. Benedix, K. Servis, D. Baratoux, L. S. Doucet, A. Rajšic, H. a. R. Devillepoix, P. A. Bland, M. C. Towner, E. K. Sansom, K. Miljković, The Tharsis mantle

source of depleted shergottites revealed by 90 million impact craters. *Nat Commun*. **12**, 6352 (2021).

51. R. Wieler, L. Huber, H. Busemann, S. Seiler, I. Leya, C. Maden, J. Masarik, M. M. M. Meier, K. Nagao, R. Trappitsch, A. J. Irving, Noble gases in 18 Martian meteorites and angrite Northwest Africa 7812—Exposure ages, trapped gases, and a re-evaluation of the evidence for solar cosmic ray-produced neon in shergottites and other achondrites. *Meteoritics & Planetary Science*. **51**, 407–428 (2016).

52. K. Hirose, Y. Fei, Y. Ma, H.-K. Mao, The fate of subducted basaltic crust in the Earth's lower mantle. *Nature*. **397**, 53–56 (1999).

53. A. Takenouchi, A. Yamaguchi, T. Mikouchi, A Newly Found Unique Shergottite Asuka 12325: Comparison in Petrology and Shock Metamorphism with Other Poikilitic Shergottites, Lunar and Planetary Science Conference LI, 1326 (2020).

54. J. D. Piercy, J. C. Bridges, L. J. Hicks, J. L. MacArthur, R. C. Greenwood, I. A. Franchi, Terrestrial alteration mineral assemblages in the NWA 10416 olivine phyric shergottite. *Geochimica et Cosmochimica Acta*. **280**, 26–45 (2020).

55. T. J. Ahrens, C. F. Petersen, J. T. Rosenberg, Shock compression of feldspars. *J. Geophys. Res.* **74**, 2727–2746 (1969).

56. M. E. Kipp, R. J. Lawrence, WONDY V: A one-dimensional finite-difference wave-propagation code. *NASA STI/Recon Technical Report N*. **83** (1982)

57. A. Navrotsky, R. Hon, D. F. Weill, D. J. Henry, Thermochemistry of glasses and liquids in the systems $CaMgSi_2O_6$-$CaAl_2Si_2O_8$-$NaAlSi_3O_8$, SiO_2-$CaAl_2Si_2O_8$-$NaAlSi_3O_8$ and SiO_2-Al_2O_3-CaO-Na_2O. *Geochimica et Cosmochimica Acta*. **44**, 1409–1423 (1980).

58. M. B. Boslough, S. M. Rigden, T. J. Ahrens, Hugoniot equation of state of anorthite glass and lunar anorthosite. *Geophysical Journal of the Royal Astronomical Society*. **84**, 455–473 (1986).

59. R. G. McQueen, S. P. Marsh, J. N. Fritz, Hugoniot equation of state of twelve rocks. *J. Geophys. Res.* **72**, 4999–5036 (1967).

60. C. D. K. Herd, E. L. Walton, C. B. Agee, N. Muttik, K. Ziegler, C. K. Shearer, A. S. Bell, A. R. Santos, P. V. Burger, J. I. Simon, M. J. Tappa, F. M. McCubbin, J. Gattacceca, F. Lagroix, M. E. Sanborn, Q.-Z. Yin, W. S. Cassata, L. E. Borg, R. E. Lindvall, T. S. Kruijer, G. A. Brennecka, T. Kleine, K. Nishiizumi, M. W. Caffee, The Northwest Africa 8159 martian meteorite: Expanding the martian sample suite to the early Amazonian. *Geochimica et Cosmochimica Acta*. **218**, 1–26 (2017).

61. R. G. Berman, Internally-consistent thermodynamic data for minerals in the system Na_2O-K_2O-CaO-MgO-FeO-Fe_2O_3-Al_2O_3-SiO_2-TiO_2-H_2O-CO_2. *Journal of petrology*. **29**, 445–522 (1988).

62. M. A. Bouhifd, P. Besson, P. Courtial, C. Gérardin, A. Navrotsky, P. Richet, Thermochemistry and melting properties of basalt. *Contrib Mineral Petrol*. **153**, 689–698 (2007).

63. T. J. Ahrens, J. D. Okeefe, "Equations of state and impact-induced shock-wave attenuation on the moon" in *Impact and Explosion Cratering: Planetary and Terrestrial Implications* (Pergamon, New York, 1977), 639–656

Acknowledgments

The authors thank Dr. Junko Isa for characterizing the initial sample of Saddleback basalt and Michael Burns and Russel Oliver for expert technical help with the shock wave experiments. Dr. Koeberl and two anonymous reviewers are thanked for their constructive comments.

Funding:

This work was funded by NASA award 80NSSC18K0532 to JH, NSF award 1947616 to PDA and NASA award 80NM0018F0612 to YL. Caltech-JPL President's and Director's Fund partially supported this work. Shock wave experiments performed in the Lindhurst Laboratory for Experimental Geophysics at Caltech are supported by NSF awards 1725349 and 1829277. A portion of this project was performed at Jet Propulsion Laboratory, managed by California Institute of Technology under a contract with NASA.

Author contributions:

Conceptualization: JH, PDA, YL. Methodology: PDA, JH, YL. Investigation: JH, YL, PDA, CM. Supervision: PDA, YL. Writing—original draft: JH. Writing—review & editing: JH, PDA, YL, CM.

Competing interests: All other authors declare they have no competing interests.

Data and materials availability: All data needed to evaluate the conclusions in the paper are present in the paper and/or the Supplementary Materials.

Figures and Tables

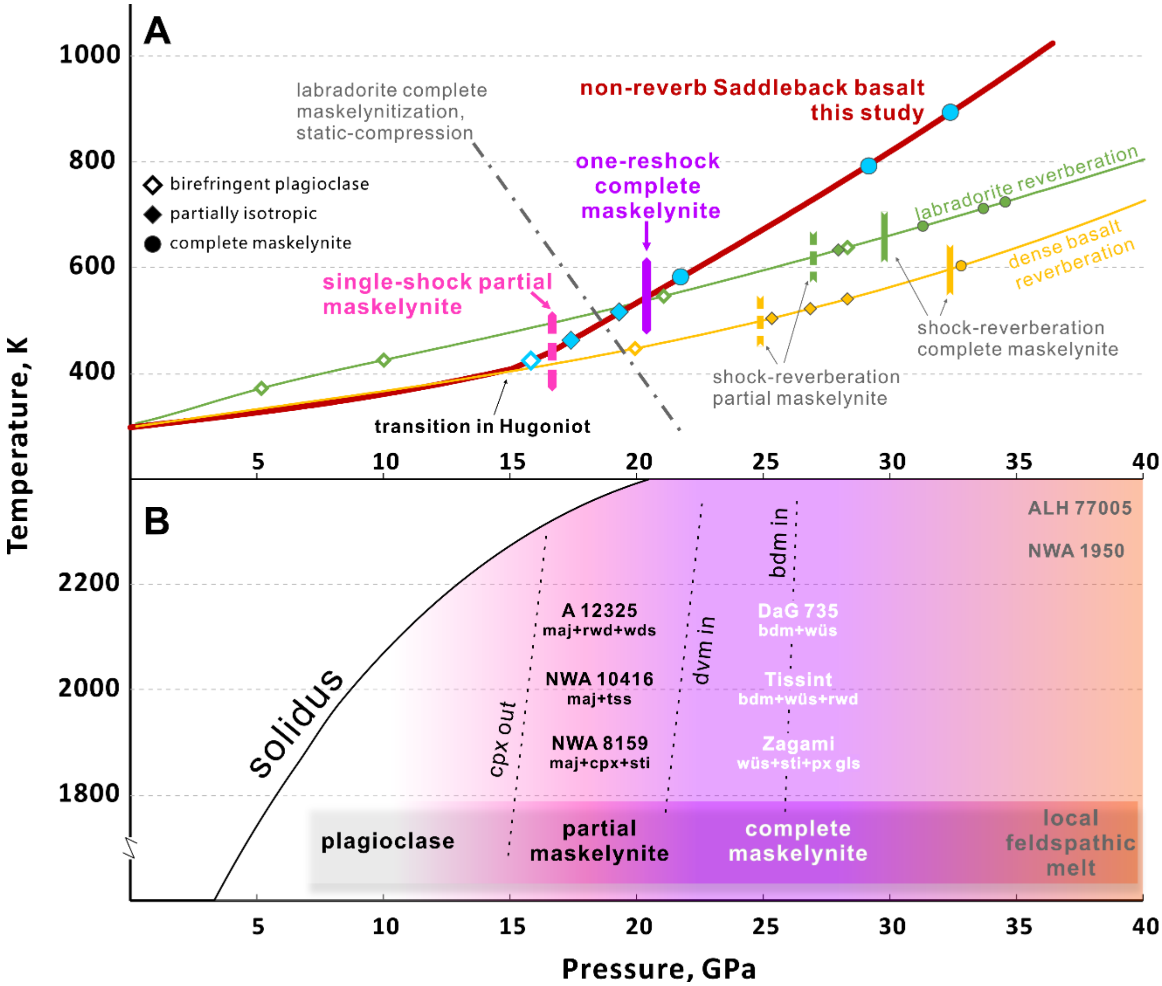

Fig. 1. Pressure-temperature (*P-T*) of maskelynite formation in experiments and Martian meteorites. (**A**) Solid curves are P-T estimates of shock experiments. The curve of Saddleback basalt (An_{65} phenocrysts) is from this study (dark red curve); the sharp change in slope corresponds to the phase change to a denser state. The interpolated thresholds for partial and complete maskelynitization are indicated by the pink-dashed and purple-solid vertical markers on the curve. The curves for single An_{65} labradorite crystal (green) and dense basalt with An_{68} labradorite (yellow) show *P-T* conditions calculated from data of reverberating recovery experiments (*11–13*, *37*) and corresponding maskelynitization thresholds (vertical dash and solid markers). Open diamond, solid diamond and solid circle on each curve indicate birefringent plagioclase, partial and full maskelynite, respectively, for the set of experiments. The tilted dot-dash line is the labradorite-maskelynite phase boundary from static compression (*21*). (**B**) Previously inferred stability fields of mineral assemblages in various shergottites, including ringwoodite (rwd), wadsleyite (wds), majorite (maj), stishovite (sti), tissintite (tss), clinopyroxene (cpx), davemaoite (dvm), bridgmanite (bdm) and ferropericlase (fp) (*16*, *17*, *52–54*). The vertical positions are schematic because shocked meteorites experience complex, heterogeneous, evolving temperature conditions. ALH 77005 and NWA 1950 do not contain HP minerals but commonly have quenched feldspar glass (*18*). The pink-purple-orange background colors indicate plagioclase-maskelynite-melt transition from this study.

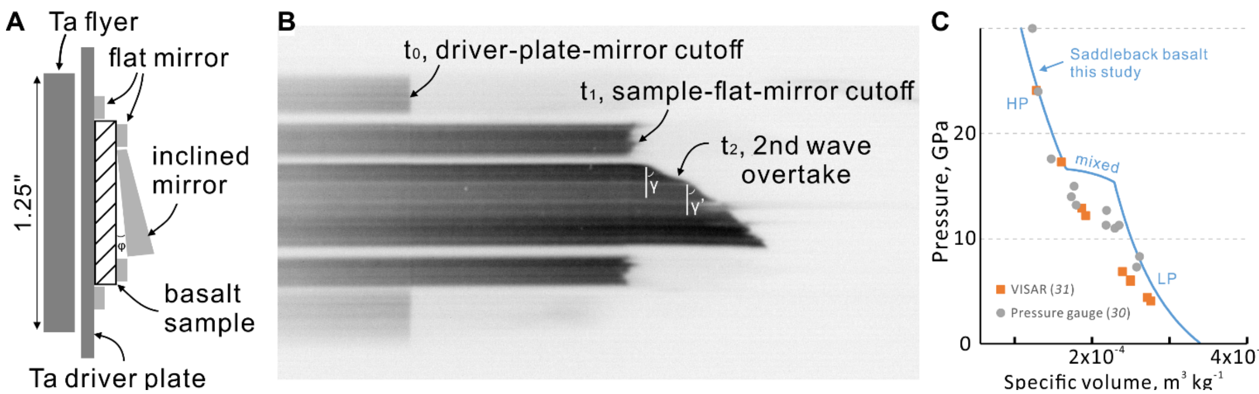

Fig. 2. Setup and results of Hugoniot EoS measurement of Saddleback basalt. (**A**) Ta flyer and target assembly consisting of Ta driver plate, basalt sample disc and mirrors silvered on the front (left) side to reflect light to streak camera. Flyer-driver-sample sizes are to scale. (**B**) Color-inverted streak camera image, with time increasing to the right and vertical axis corresponding to position across sample as shown in (A). Total streak duration is 4 μs. The end of each dark streak shows a shock wave striking the mirror at that position and time. t_0 and t_1 correspond to the time of shock wave entering the sample and reaching the back of the sample. Inclined-mirror cutoff indicates the timing of decompressed material hitting the mirror at free-surface velocity, determined by slope angle γ. The change in slope at time t_2 is caused by a second shock wave overtaking the first arriving wave. Irregular cutoffs result from the heterogeneity of porosity and mineralogy of the basalt at mm scale. (**C**) The fitted Hugoniot in pressure-volume space. The piecewise curve indicates low-pressure (LP), mixed-phase, and high-pressure (HP). Curvature of the LP regime does not affect the pressure calculations for recovery shots. The Hugoniot data of Kinosaki basalt measured by piezoresistive gauges (*30*) and VISAR (*31*) show similar complication although not exactly matching Saddleback basalt (Fig. S2-3).

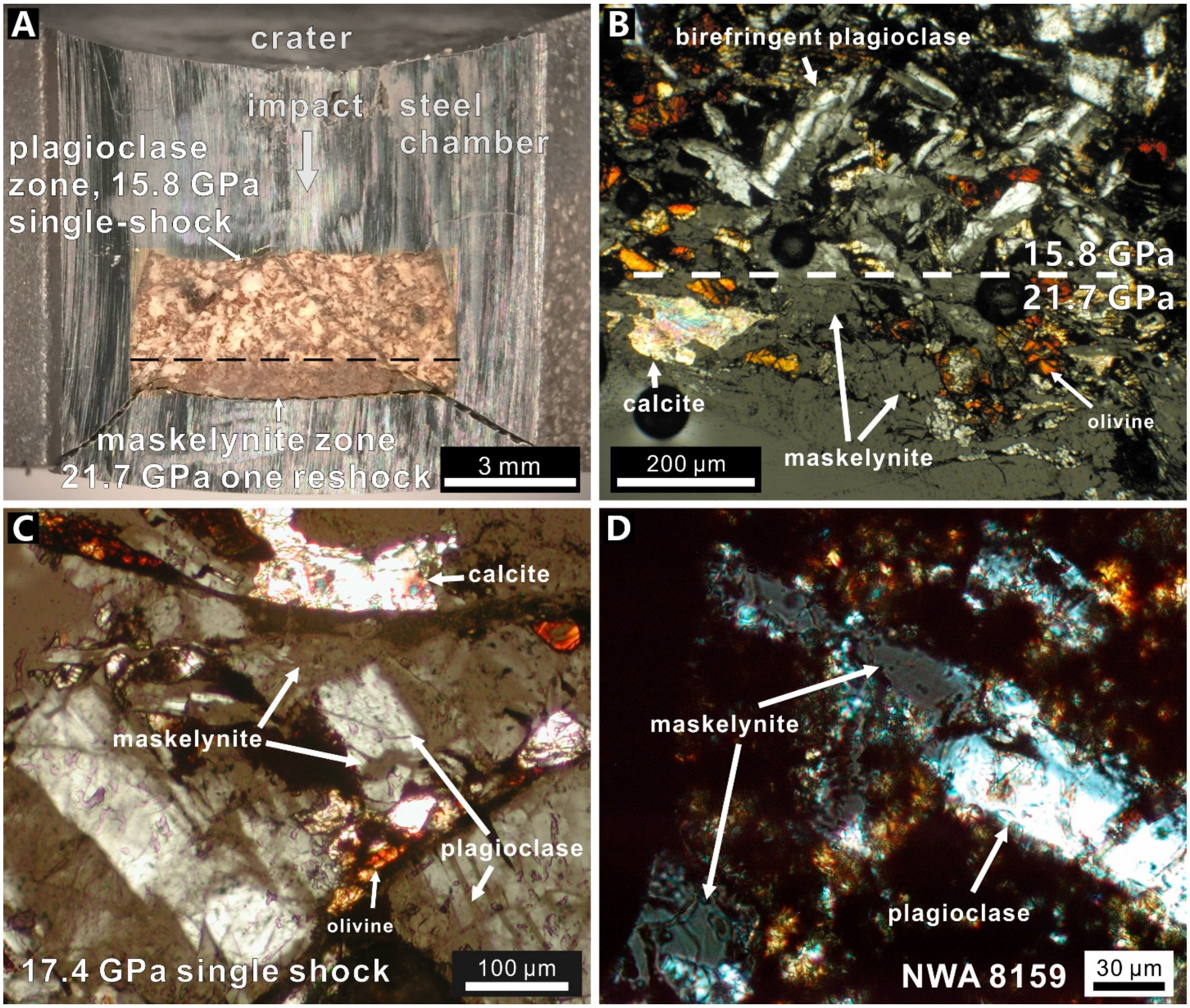

Fig. 3. Photos of shock-recovered Saddleback basalt. (**A**) Thick section of S1240 sample in steel chamber with a region that experienced a single shock to 15.8 GPa and a region that experienced one reflected shock to 21.7 GPa, with boundary indicated by a dashed line. Plagioclase in the single-shocked region shows its original white color but the maskelynite in the reshocked region is transparent and displays deformed shapes. Two oblique fractures propagated from the deformed thread of the rear chamber cap. (**B**) Nonorthogonal (87-88°) cross-polarized light (xpl) micrograph of the pressure-transition region of S1240 in thin section. All plagioclase grains transformed to maskelynite (isotropic) in the reshocked zone. (**C**) Nonorthogonal xpl image of partial maskelynite in region of recovered sample S1244 that experienced single shock to 17.4 GPa. Plagioclase grains are 30-40% maskelynitized. The non-isotropic portions show lower birefringence than single-shocked grains in S1240. (**D**) Nonorthogonal xpl image of partial maskelynite in shergottite NWA 8159 (*17*).